Simulation of boundary condition influence in a second-order ferroelectric phase transition

Wenwu Cao[a)]
Department of Mathematics and Materials Research Laboratory, The Pennsylvania State University, University Park, Pennsylvania 16802

Simon Tavener
Department of Mathematics, The Pennsylvania State University, University Park, Pennsylvania 16802

Shumao Xie
Materials Research Laboratory, The Pennsylvania State University, University Park, Pennsylvania 16802

(Received 22 March 1999; accepted for publication 10 August 1999)

Using a two-dimensional Ginzburg–Landau model and the finite-element computational method, we have calculated stable domain configurations resulting from a second-order ferroelectric phase transition for a finite-sized system. The boundary conditions applied here correspond to fully charge compensated situations, either by surface electrodes or by the injection of charges (or defects) near the sample surface. The domain wall thickness of a finite system without surface electrodes was found to become thinner as it approaches sample surfaces. This is distinctively different from that of an infinite system for which a planar wall assumption can be used. The orientation of the macroscopic polarization of a finite system without surface electrodes was found to be determined by its aspect ratio. A size effect was observed when all the dimensions were reduced simultaneously. The relaxation process in the formation of domains and the switching process have also been simulated for charge neutral boundary conditions using a time dependent Ginzburg–Landau model. The simulation results verified that the surfaces are the favored nucleation sites for domain switching. © *1999 American Institute of Physics.* [S0021-8979(99)02522-0]

I. INTRODUCTION

Many physical properties of technologically important materials are determined by mesoscopic structures, such as domains and domain walls. For example, it has been determined experimentally that 70% of the dielectric and piezoelectric contribution in ferroelectric materials can be attributed to domain related activities.[1,2] An understanding of the formation processes of such mesoscopic structures is therefore crucial for designing and engineering better active materials. A great deal of effort has already been invested in this area, including first principle calculations, analytical approaches, and computer simulations,[3–7] and some notable successes have been achieved. However, analytical solutions are generally limited to quasi-one dimensional (1D) solutions, and most simulations have used periodic boundary conditions for reasons of computational efficiency. While these procedures may be appropriate when dealing with very large systems, the growing trend towards making smaller and smaller particles and thin films provides new challenges. In particular, size effects have attracted more and more attention in the past few years due to the fast growing field of thin films and microelectromechanical devices. Static analyses using an isotropic surface layer for particles and a one-dimensional model for thin films have been carried out by several authors for ferroelectrics.[8–11]

An established way of treating finite sized materials in simulation studies is to use layered vacuum–material–vacuum composites and periodic boundary conditions. The periodic boundary conditions allow the use of computational efficient fast Fourier transform techniques. While this approach may be appropriate to approximate free boundary conditions if the volume of the vacuum region is sufficiently large, it cannot describe practical situations in which external boundary conditions are prescribed. For this reason, it is necessary to explore models that allow the direct application of external boundary conditions and numerical methods that make the computation size manageable. In this article we have used scale normalization and the finite-element method in an effort to simulate domain formation in a finite ferroelectric system with high computational efficiency. We focus on the effects of surfaces in a finite system under prescribed boundary conditions. In order for the problem to be well posed, full electric charge compensation is assumed, which can be achieved either through surface electrodes or by injection of charges (or the distribution of charged defects) to neutralize the polarization gradient near the sample surfaces.

The time evolution of the domain pattern under specified boundary conditions was also investigated using a time-dependent Ginzburg–Landau (TDGL) theory.[12] A variable time-step integration technique was used that allows the energy minima to be obtained efficiently. In this technique, the time step was increased by several orders of magnitude as the system approached equilibrium. Without prescribed polarization at the surfaces, a single domain state was found to be the global energy minimum, as expected, since domain walls contain positive energy and will be driven out of the

a)Electronic mail: caomath.psu.edu

system without surface pinning. Because there is no depolarization energy for the neutralized system, multidomain states can exist only with prescribed polarization at the boundaries. For the case of charge injection near the surface region, polarization became geometry dependent and the aspect ratio was found to break the orientational degeneracy of the system due to the gradient energy. Our model does not involve the introduction of a surface layer; the surface effect is intrinsic and anisotropic.

In this preliminary exploration, we did not include the strain coupling in order to isolate the effects of electrical boundary conditions. The model system has a square to rectangular phase transition [which may also be used to describe the tetragonal to orthorhombic phase transition in a three-dimensional (3D) system with the tetragonal dimension fixed], and a square to rhombic transition.

An outline of this article is as follows. In Sec. II we introduce the model, in Sec. III we discuss the effects of boundary conditions on the formation of domains in equilibrium states, and in Sec. IV we discuss the time evolution of domain processes.

II. GINZBURG–LANDAU MODEL FOR SQUARE–RECTANGULAR AND SQUARE–RHOMBIC FERROELECTRIC PHASE TRANSITIONS

The model system we investigated is a two-dimensional (2D) analog of the perovskite structure with the positive and negative ions sitting at the center and corner of a square unit cell, respectively. The symmetry of the high temperature paraelectric phase is square. We assume that the system undergoes a proper second-order ferroelectric phase transition so that the system can be described by a fourth-order Ginzburg–Landau theory. Using the polarization as the order parameter, the free energy density for a second-order phase transition can be written as

$$\begin{aligned} f=&\alpha_1(P_1^2+P_2^2)+\alpha_{11}(P_1^2+P_2^2)^2+\alpha_{12}P_1^2P_2^2 \\ &+d_1\left[\left(\frac{\partial P_1}{\partial x_1}\right)^2+\left(\frac{\partial P_2}{\partial x_2}\right)^2\right]+d_2\left(\frac{\partial P_1}{\partial x_1}\right)\left(\frac{\partial P_2}{\partial x_2}\right) \\ &+d_3\left[\left(\frac{\partial P_1}{\partial x_2}\right)^2+\left(\frac{\partial P_2}{\partial x_1}\right)^2\right], \end{aligned} \tag{1}$$

where only the first coefficient $\alpha_1=\alpha_0(T-T_c)(\alpha_0>0)$ is temperature dependent; all the other coefficients are assumed to be independent of the temperature. Unlike previously proposed models, the gradient energy in Eq. (1) is anisotropic.

Minimizing the free energy density described by Eq. (1) gives three types of stable homogeneous solutions as listed below.

A. Solution 1

For temperature $T>T_c,(\alpha_1>0)$ a paraelectric solution exists for which

$$P_1=P_2=0. \tag{2}$$

The symmetry of this paraelectric state is square.

B. Solution 2

For temperature $T<T_c(\alpha_1<0)$, if $\alpha_{11}>0$ and $\alpha_{12}>0$, a rectangular ferroelectric phase is stable, and has four variants: $(\pm P_R,0)$ and $(0,\pm P_R)$, where the spontaneous polarization P_R is given by

$$P_R=\sqrt{\frac{-\alpha_1}{2\alpha_{11}}}. \tag{3}$$

The symmetry of this low-temperature state is rectangular.

C. Solution 3

For temperature $T<T_c(\alpha_1<0)$, if $\alpha_{11}>0$ and $-4\alpha_{11}<\alpha_{12}<0$, a rhombic ferroelectric phase is stable. It also has four variants: $(\pm P_{Rh},\pm P_{Rh})$, with the spontaneous polarization component, P_{Rh}, given by

$$P_{Rh}=\sqrt{\frac{-\alpha_1}{4\alpha_{11}+\alpha_{12}}}. \tag{4}$$

In order to compute an inhomogeneous static solution below T_c, one needs to solve the Euler equations,[2,3,13] that in this case are two coupled second-order nonlinear partial differential equations of the following form:

$$\begin{aligned} &2d_1P_{1,11}+d_2P_{2,21}+2d_3P_{1,22} \\ &\quad=2\alpha_1P_1+4\alpha_{11}(P_1^2+P_2^2)P_1+2\alpha_{12}P_1P_2^2, \end{aligned} \tag{5a}$$

$$\begin{aligned} &2d_1P_{2,22}+d_2P_{1,12}+2d_3P_{2,11} \\ &\quad=2\alpha_1P_2+4\alpha_{11}(P_1^2+P_2^2)P_2+2\alpha_{12}P_2P_1^2. \end{aligned} \tag{5b}$$

Under a quasi-1D approximation, these equations can be reduced to two coupled ordinary differential equations which could be addressed by the method given in Refs. 4 and 14. In this article, however, we will directly solve this set of partial differential equations using the finite-element method (see the Appendix) with several prescribed boundary conditions.

For demonstration purposes we only study the case of $\alpha_{12}>0$, for which the rectangular phase is stable. The case of $\alpha_{12}<0$ has a very similar physical appearance if one rotates the coordinate system 45°. For generality, Eq. (5) is converted into dimensionless form by making the following substitutions:

$$\begin{pmatrix}P_1\\P_2\end{pmatrix}=P_R\begin{pmatrix}u\\v\end{pmatrix}, \tag{6}$$

$$\begin{pmatrix}x_1\\x_2\end{pmatrix}=\sqrt{\frac{d_1}{-a\alpha_1}}\begin{pmatrix}\xi\\\eta\end{pmatrix}, \tag{7}$$

where $a(>0)$ is a dimensionless scaling factor included here to give the flexibility to adjust the strength of the gradient energy with respect to that of the Landau energy. In addition, we define three new dimensionless coefficients specifying the anisotropy of the gradient energy and the coupling strength between different polarization components,

$$b=a\frac{d_2}{2d_1}, \tag{8a}$$

$$c = a\frac{d_3}{d_1}, \tag{8b}$$

and

$$d = \frac{\alpha_{12}}{2\alpha_{11}}. \tag{8c}$$

The final dimensionless form of Eq. (5) is

$$a u_{\xi\xi} + b v_{\xi\eta} + c u_{\eta\eta} = -u + u^3 + (1+d) u v^2, \tag{9a}$$

$$a v_{\eta\eta} + b u_{\xi\eta} + c v_{\eta\eta} = -v + v^3 + (1+d) v u^2. \tag{9b}$$

For a given system, the gradient coefficients *a*, *b*, and *c* may be determined by inelastic neutron scattering experiments,[14,15] while the nonlinearity coefficient, *d*, can be obtained from measurements of the nonlinear dielectric constant.[16] In the current 2D model system, we will investigate a particular set of normalized constants to provide the general trend of the solutions. For any specific material one could apply the procedure described in this article to obtain the inhomogeneous solutions after determining these parameters from experiments.

The coupled partial differential equations, Eqs. (9a) and (9b), were solved using the finite-element method described in the Appendix. Nine node quadrilateral elements were used in our calculations and the density of the elements in any given direction reflects the real dimension in that direction. The dimensions of the system were normalized to 1 so that the computational procedure could be applied to any size through a scaling factor. The scaling factor was also used to convert the simulation results back to the original dimensions after the problem was solved in the normalized system.

III. EFFECTS OF BOUNDARY CONDITIONS ON THE FORMATION OF DOMAIN STATES

A. Surface electrodes versus charge injection

The natural boundary conditions arising in the finite-element solution technique correspond to a system with surface electrodes that is short circuited during the phase transition. The depolarization field is screened by the free charge so that the magnitude of the polarization can be maintained as a constant throughout the sample. Under this circumstance, a monodomain state is the global energy minimum.[17] Our model simulation quickly converges to such a single domain state. The initial guess used when solving Eq. (9) was generated by the time-dependent model described in Sec. IV.

The boundary condition $\mathbf{P}\cdot\mathbf{n}=0$ corresponds to the situation of charge injection (or charged defect concentration) near the surface region. This case reflects many realistic situations in which a surface layer develops with reduced polarization.[8–11] We found a strong aspect ratio effect when this boundary condition was applied. The polarization of the stable configuration was always parallel to the long dimension. In other words, the dimensional difference breaks the symmetry degeneracy of the two pairs of solutions under this boundary condition. Only at the critical aspect ratio of 1 do all four possible solutions (with orientation ⟨10⟩) have equal chances of forming.

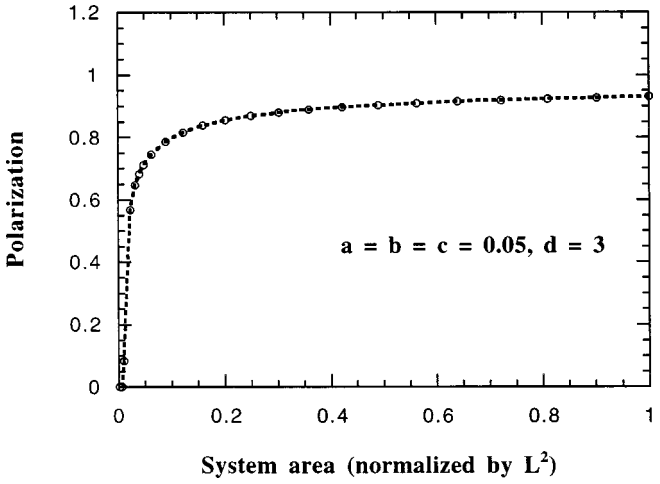

FIG. 1. Reduced effective polarization near surfaces causes a size effect. There is a critical size at which the effective polarization vanishes. The parameters used in the calculations are $a=b=c=0.05$ and $d=3$.

The implication of this result is that the natural state for a free standing thin film without surface electrodes should have polarization lying in the plane, although the net polarization would still be zero due to the in-plane random orientation. We must emphasize that this conclusion is only true for a free standing film, otherwise, the polarization orientation will be determined by the constraints originating from lattice constant mismatch between the film and the substrate, which is beyond the scope of this model system.

B. Size effects in a single domain system with P.n=0 boundary conditions

Size effects become increasingly important as material systems become smaller and smaller. Many experimental results showed that material properties degrade as the size decreases.[18–23] To determine this size effect, we used a square system of size $L\times L$ and continuously reduced the value of L. The net effective polarization is shown in Fig. 1. A critical size is clearly shown in the computational results although the actual value of the critical size depends on material parameters, particularly on the gradient coefficients. Our results are similar to those reported earlier by introducing an isotropic surface layer with reduced polarization.[11] The difference is that we did not make the assumption of a surface layer, but, rather, incorporated the gradient anisotropy and boundary conditions. Our model predicts strong size effects only when all the dimensions are being reduced at the same time. If the reduction is only in one of the dimensions, such as in thin films, the polarization can still be formed in the other larger dimension unless a reduced polarization layer is introduced.

Generally speaking, this critical size is directly related to the strength of the nonlocal interaction of the polarization, i.e., the amplitude of the polarization gradient coefficients.

C. Twin structures and their size dependence

Under the quasi-1D approximation, a single twin solution can be derived using the method described in Refs. 4

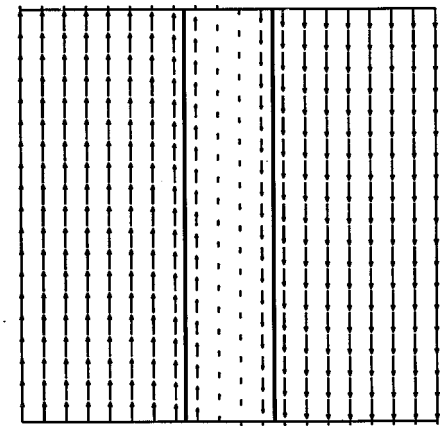

FIG. 2. Equilibrium configuration of a 180° twin with top and bottom surfaces electroded and the left and right boundaries being prescribed with the boundary condition of ± 1 for the vertical component and zero for the horizontal component, respectively.

and 14 for infinite systems. Here, we study a finite system with surface electrodes at the top and the bottom surfaces and prescribe the polarization on the two side surfaces. The 180° twin and 90° twin solutions are shown in Figs. 2 and 3, respectively. In order to compare them with the quasi-1D solutions of Ref. 4, we look at the solution along the middle of the vertical dimension in the 2D structure (maximum domain wall width). The contour lines in Figs. 2 and 3 represent the position where the polarization amplitude has reached 79%[$=\tanh(1)$] of its maximum value. We take the region in between the two contour lines as the ''domain wall.'' One can see that the domain wall thickness for the 90° twin decreases as it approaches the top and bottom surfaces. The corresponding parameters used for the simulation are given in the Figs. 2 and 3 captions.

The results imply that the quasi-1D assumption (plane wall assumption) is inadequate if the systems is very small. As shown in Fig. 3, the symmetry inside a 90° wall is lower

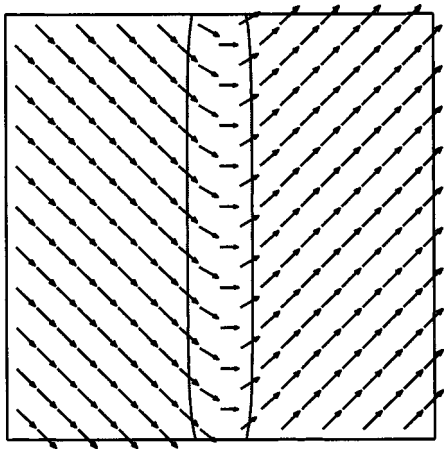

FIG. 3. 2D system with the dimensions parallel to [11] and $[\bar{1}1]$. The equilibrium configuration of a 90° twin is obtained with the top and bottom surfaces electroded and the left and right boundaries prescribed with the boundary condition of the polarization pointing to [10] and [01] directions, respectively (45° with respect to the surface orientations). The contour lines illustrate the change of domain wall width from the center to the top and bottom surfaces.

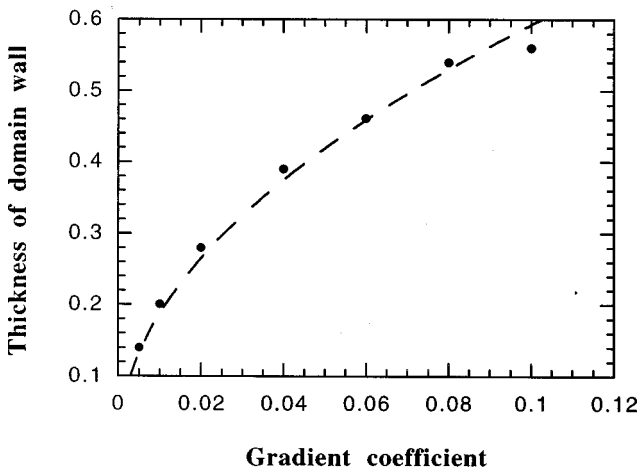

FIG. 4. Dependence of the domain wall thickness on the amplitude of the gradient coefficients. We chose $a=b=c$ for convenience to compare these results with that of 1D models. The dashed line is the square-root relationship obtained from a 1D model.

than that of the single domain regions, and the direction of the polarization at the center of the domain wall is along the diagonal direction of the unit cell (i.e., 45° from the single domain regions). In Fig. 4 we plot the domain wall thickness measured at the center of the simulated systems versus the gradient coefficient (for convenience, we have set a $a=b=c$) while keeping all the other parameters fixed. The dashed line is the square root relationship predicted by the 1D model, and the dots are our computational results. One can see that the simulation results agree well with the 1D analysis even when the wall thickness reached 50% of the system size. The deviation for the large gradient coefficient is caused by the boundary constraints to the domain wall.

IV. RELAXATION IN DOMAIN FORMATION AND FIELD INDUCED SWITCHING PROCESS

A time-dependent Ginzburg–Landau model can provide information about the time evolution of domain formation from a quenched state below T_c. The TDGL used here is a relaxation equation for a nonconserved order parameter, corresponding to model A described by Hohenberg and Halperin.[12] Simulations using periodic boundary conditions have revealed that the domain coarsening slows down considerably upon approaching equilibrium.[6,7] In order to simulate a finite system in direct space within a realizable time scale without having to invoke the periodic boundary condition, we used a variable time-step scheme that is described in the Appendix. The computational efficiency of this method allows us to perform real space finite size simulations and to explore the effects of boundary conditions.

The master equation used here is of the same form as model A described in Ref. 12:

$$\frac{\partial P_i}{\partial t} = -\Gamma \frac{\delta F}{\partial P_i} + R(r,t) + \Gamma E_i, \quad (i=1,2), \tag{10}$$

where Γ is the kinetic coefficient, F is the volume integration of Eq. (1), $R(r,t)$ represents the Gaussian random noise, and E_i is the external electric field.

When carrying out the simulation, $R(r,t)$ [$<10^{-4}$], was only used for initiating the nucleation process at the beginning from a paraelectric state, and was neglected at later stages because it does not affect the ultimate equilibrium states. Using a normalized time τ and a frequency Ω defined by

$$\tau = -2\alpha_1 \Gamma t, \tag{11}$$

$$\Omega = \frac{\omega}{-2\alpha_1 \Gamma}, \tag{12}$$

and substituting the dimensionless variables and coefficients defined by Eqs. (6)–(8), we can derive the normalized governing equations for the temporal evolution of the normalized polarization under an external AC electric field.

$$u_{,\tau} = a u_{,\xi\xi} + b v_{,\xi\eta} + c u_{,\eta\eta} + u - u^3 - (1+d) u v^2 - e_\xi \cos(\Omega \tau), \tag{13a}$$

$$v_{,\tau} = a v_{,\xi\xi} + b u_{,\xi\eta} + c v_{,\eta\eta} + v - v^3 - (1+d) v u^2 - e_\eta \cos(\Omega \tau), \tag{13b}$$

where $e = E/(-2\alpha_1 P_R)$ is the amplitude of the dimensionless form of the external electric field.

Figure 5 shows the domain formation process with **P.n** $=0$ boundary conditions from a quenched state below T_c. The simulation was initiated from a small amplitude random disturbance. Because the amplitude is too small to see at the beginning, we have multiplied the magnitude of the local polarization vectors by an amplification factor. For example, the amplitude of the polarization vectors drawn in Fig. 5(d) has been amplified 80 000 times. It is interesting to see that the amplitude of local polarization first shrank to almost zero before re-nucleating into small clusters which grew into many small domains. As the coarsening progressed, the dominant domains grew at the expense of the smaller ones. The final equilibrium state was determined by the nucleus whose local polarization amplitude reached the equilibrium value first. In order to compare the efficiency of the variable time step finite-element method used in our simulation, we define a unified dimensionless time $\Delta t_0 = 10^{-3}$ as the unit. Using this unit as a measure, the polarization evolution from Figs. 5(a)–5(f) will take 42 000 time steps. While using the variable time step method, it only took 140 variable time steps to reach the equilibrium state in Fig. 5(f), and this represents a tremendous saving of computational time. The time steps of both measures are given in the Fig. 5 caption.

Figure 6 is another simulation sequence with surface electrode boundary conditions. In this case, the equilibrium was reached in 14 000 time steps in the unit of Δt_0, but our simulation only required 110 variable time steps. It is important to point out that our simulation showed no size effect with the electroded surfaces in terms of the polarization for this case. This is the main difference between our model and previous models, which assumed a surface layer with reduced polarization.

Letting $\Omega \to 0$ in Eq. (13) we can simulate the quasistatic switching process. It is much easier to form nuclei of the opposite domain near the surface region because of the influence of the boundary conditions. In our model the switching does not happen homogeneously in the whole system but, rather, nucleates at the surfaces and then progresses via the movement of domain walls. The time evolution of the domain switching process for a 90° twin structure is illustrated in Fig. 7. The net polarization of the twin was pointing to the right before application of an electric field, which is opposite to the initial polarization direction. Two domain walls formed near the left and the right surface regions at the beginning, then they moved toward each other and finally annihilated one another in the middle of the structure, forming a reversed twin with the effective polarization pointing to the left (the field direction). It is interesting to see that a swirl

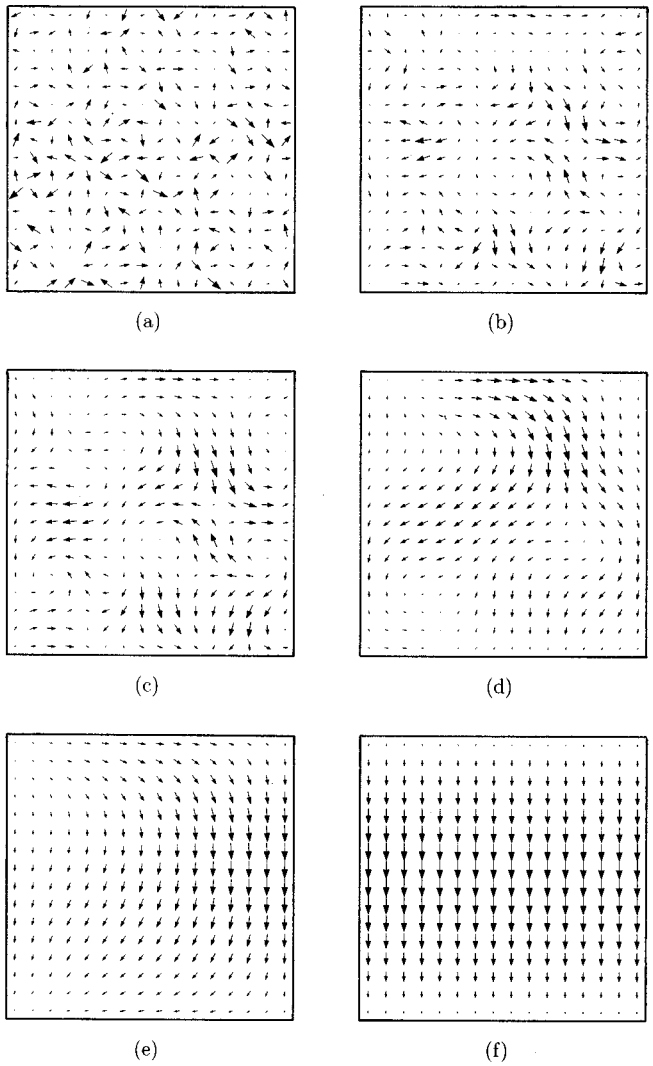

FIG. 5. Time evolution of the domain formation process from a random to a single domain state for the **P.n**$=0$ boundary condition. (a) $\tau=0$ and the amplitude of the local polarization has been amplified 3333 times; (b) 30 variable time steps$=35\Delta t_0$, and the amplitude of the local polarization has been amplified 20 000 times; (c) 35 variable time steps$=97\Delta t_0$ and the amplitude of the local polarization has been amplified 20 000 times; (d) 40 variable time steps$=350\Delta t_0$, and the amplitude of the local polarization has been amplified 80 000 times; (e) 45 variable time steps$=1600\Delta t_0$, and the amplitude of the local polarization has been amplified 6667 times; (f) 140 variable time steps$=42\,000\Delta t_0$ and there was no amplification at the local polarization vectors. The parameters used in the simulation are $a=0.045$, $b=0.055$, $c=0.05$, $d=2.5$, and $\boldsymbol{e}=\mathbf{0}$.

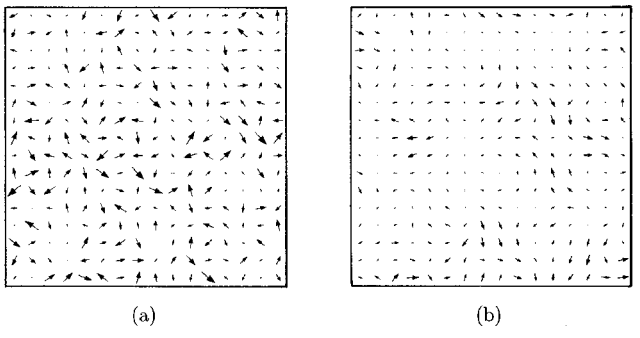

FIG. 6. Time evolution of the domain formation process from a random to a single domain state for a system with shortened surface electrodes (a) $\tau=0$ and the amplitude of the local polarization has been amplified 4000 times; (b) 35 variable time steps $=78\Delta t_0$ and the amplitude of the local polarization has been amplified 24 000 times; (c) 40 variable time steps $=230\Delta t_0$ and the amplitude of the local polarization has been amplified 40 000 times; (d) 45 variable time steps $=780\Delta t_0$, and the amplitude of the local polarization has been amplified 40 000 times; (e) 50 variable time steps $=3300\Delta t_0$ and the amplitude of the local polarization has been amplified 600 times; (f) 110 variable time steps $=14000\Delta t_0$, and there was no amplification of the local polarization vectors. The parameters used in the simulation $a=0.06$, $b=0.04$, 0.05, $d=2$, and $\boldsymbol{e}=\mathbf{0}$.

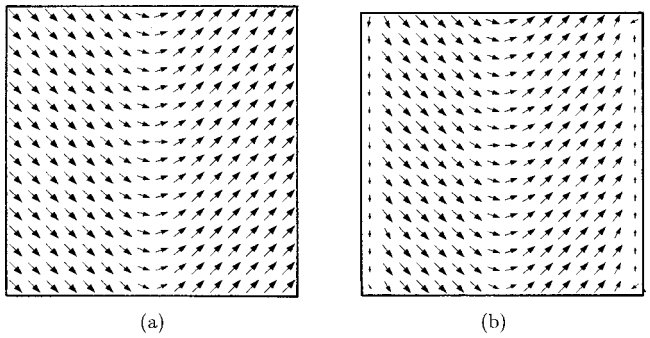

FIG. 7. Switching process of a 90° twin. The starting net polarization was pointing to the right. The time steps are (a) 0; (b) 80 variable time steps $=170\Delta t_0$; (c) 140 variable time steps $=6200\Delta t_0$; (d) 180 variable time steps $=17\,000\Delta t_0$; (e) 280 variable time steps $=30\,000\Delta t_0$; (f) 330 variable time steps $=37\,000\Delta t_0$. The parameters used for the simulations are $a=0.014$, $b=0.01$, $c=0.012$, $d=2.0$, and field amplitude $\boldsymbol{e}=10^{-2}$. The switching process started at both surfaces on the left and right sides and propagates to the interior. Two domains walls form near the surfaces and they move toward each other until annihilation.

pattern developed in Fig. 7(d). Such a phenomenon can occur because our current model does not include elastic strain coupling. The walls are expected to be planar while moving under the force of the electric field if the elastic constraints are included.

V. SUMMARY AND CONCLUSIONS

A 2D ferroelectric model system has been investigated using a finite-element technique combined with a variable time step numerical scheme. The unique feature of our model is the introduction of the anisotropic gradient energy which is compatible with the structural symmetry. We also directly solved the coupled partial nonlinear differential equations rather than trying to reduce the problem to one dimension. Due to the high efficiency of the numerical method, we were able to simulate both the equilibrium polarization configuration and the temporal evolution of the local polarization formation in a finite system with different boundary conditions. The simulation results agree well with all the known facts for a second-order ferroelectric phase transition, such as size effects, switching via surface nucleation–domain wall movement, and aspect ratio effects. In particular, we have demonstrated the temporal evolution of domain formation and the switching process in a 90° twin system.

ACKNOWLEDGMENTS

This work was sponsored by National Science Foundation Grant No. DMS-9704714 and the ONR under MURI Grant No. N00014-96-1-1173.

APPENDIX

We used the finite-element code ENTWIFE[24] to solve the following coupled system of partial differential equations [see Eq. (13)] in a rectangular domain D:

$$u_{,\tau} = a u_{,\xi\xi} + b v_{,\xi\eta} + c u_{,\eta\eta} + u - u^3 - (1+d) u v^2 - e_\xi \cos(\Omega\tau), \tag{A1a}$$

$$v_{,\tau} = a v_{,\xi\xi} + b u_{,\xi\eta} + c v_{,\eta\eta} + v - v^3 - (1+d) v u^2 - e_\eta \cos(\Omega\tau). \tag{A1b}$$

The code ENTWIFE incorporates sophisticated parameter continuation capabilities and the ability to locate bifurcation points at which qualitative changes in the solution set occurs, making it particularly suitable to solve multiparameter problems. The numerical bifurcation techniques implemented in the code have proven to be useful to study a wide range of problems in fluid and other continuous systems.

In order to write Eqs. (A1a) and (A1b) in a form to which we can apply the standard finite-element approach (see, e.g., Refs. 25 and 26), it is convenient to introduce the notation,

$$p = \begin{pmatrix} u \\ v \end{pmatrix}, x_1 = \xi, \quad x_2 = \eta, \quad \frac{\partial}{\partial x_1} = \frac{\partial}{\partial \xi}, \quad \frac{\partial}{\partial x_2} = \frac{\partial}{\partial \xi},$$

so that

$$p_{1.l} = u_{,\xi} \quad \text{and} \quad p_{2.2} = v_{,\eta}, \quad \text{etc.}$$

First, consider the steady state problem without an external field. Let $\mathbf{f(p)}$ be a vector valued function,

$$f_i(p) = \alpha p_{i,jj} + \beta p_{j,ij} + \gamma p_{k,ki} \quad (i = 1, 2), \tag{A2}$$

where $k = 3 - i$ with a summation over the repeated index $j = 1, 2$ (but not over k). Expanding Eq. (A2) using the original variables we have

$$\mathbf{f(p)} = \begin{pmatrix} \alpha(u_{,\xi\xi} + u_{,\eta\eta}) + \beta(u_{,\xi\xi} + v_{,\xi\eta}) + \gamma v_{,\xi\eta} \\ \alpha(v_{,\xi\xi} + v_{,\eta\eta}) + \beta(u_{,\xi\eta} + v_{,\eta\eta}) + \gamma u_{,\xi\eta} \end{pmatrix} = \begin{pmatrix} (\alpha+\beta) u_{,\xi\xi} + (\beta+\gamma) v_{,\xi\eta} + \alpha u_{,\eta\eta} \\ \alpha v_{,\xi\xi} + (\beta+\gamma) u_{,\xi\eta} + (\alpha+\beta) v_{,\eta\eta} \end{pmatrix}.$$

Defining a second vector-valued function $\mathbf{g(p)}$ by

$$\mathbf{g(p)} = \begin{pmatrix} u - u^3 - (1+d) u v^2 \\ v - v^3 - (1+d) u^2 v \end{pmatrix},$$

the static problem without external field becomes

$$\mathbf{f(p)} + \mathbf{g(p)} = 0, \tag{A3}$$

provided constants α, β, and γ are related to constants a, b, and c as

$$\alpha = c, \quad \beta = a - c, \quad \gamma = b - c.$$

Let the boundary of domain D to be divided into two parts, $\partial D = \partial D_1 + \partial D_2$, where u and v are specified on ∂D_1, i.e., $\mathbf{p} = \mathbf{q}$ on ∂D_1, and are not specified on ∂D_2.

We seek a solution $\mathbf{p} \in V_q$ of Eq. (A3) where $V_q = \{\mathbf{p}: \mathbf{p} \in \mathbf{H}^1(D), \mathbf{p} = \mathbf{q} \text{ on } \partial D_1\}$. Here $\mathbf{H}^1(D)$ is the space of vector functions defined on D whose function values and first derivatives lie in $L^2(D)$. In the usual way, we construct the weak form of Eq. (A3) by taking the dot product of $\mathbf{(f+g)}$ with a (vector) test function $\mathbf{r}$, and requiring that the integral of the dot product over the domain D vanishes for all test functions $\mathbf{r} \in V_0$, where

$$V_0 \in \{\mathbf{p}: \mathbf{p} \in H^1(D_1): \mathbf{p} = 0 \text{ on } \partial D_1\}.$$

Summing over the repeated indexes i and j, notice that

$$\alpha \frac{\partial}{\partial x_j}(p_{i,j} r_i) + \beta \frac{\partial}{\partial x_j}(p_{j,i} r_i) + \gamma \frac{\partial}{\partial x_j}(p_{k,k} r_j) = \alpha p_{i,jj} r_i + \beta p_{j,ij} r_i + \gamma p_{k,kj} r_i + \alpha p_{i,j} r_{i,j} + \beta p_{j,i} r_{i,j} + \gamma p_{k,k} r_{j,i}, \tag{A4}$$

where $k = 3 - j$.

By applying the divergence theorem in the plane,

$$\int\int_D (\alpha p_{i,jj} r_i + \beta p_{j,ij} r_i + \gamma p_{k,kj} r_j) d\xi d\zeta = \int_{\partial D} (\alpha p_{i,j} r_i n_j + \beta p_{j,i} r_i n_j + \gamma p_{k,k} r_j n_i) ds - \int\int_D (\alpha p_{i,j} r_{i,j} + \beta p_{j,i} r_{i,j} + \gamma p_{k,k} r_{j,j}) d\xi d\zeta, \tag{A5}$$

where $\boldsymbol{n}$ is the outward surface normal. By including the terms in $\mathbf{g(p)}$, the weak form of the steady state equations is

$$\int\int_\Omega \{[p_1 - p_1^3 - (1+d) p_1 p_2^2] r_1 + [p_2 - p_2^3 - (1+d) p_2 p_1^2] r_2 - [\alpha p_{i,j} r_{i,j} + \beta p_{j,i} r_{i,j} + \gamma p_{k,k} r_{j,j}]\} d\xi d\zeta = 0. \tag{A6}$$

Since the test functions r_i, $i = 1,2$ vanish on ∂D_1 by construction, the ''natural'' boundary conditions that apply on ∂D_2 arise from the requirement that the boundary integral term in Eq. (A5) vanishes for all possible test functions. The natural boundary conditions on ∂D_2 are, therefore,

$$\alpha p_{1,j} n_j + \beta p_{j,1} n_1 + \gamma n_1 p_{2.2} = 0, \tag{A7a}$$

$$\alpha p_{2,j} n_j + \beta p_{j,2} n_j + \gamma n_2 p_{1,1} = 0. \tag{A7b}$$

Rectangular elements with biquadratic interpolation were used to construct finite-dimensional subspaces $V_q^h \subset V_q$ and $V_0^h \subset V_0$. The finite-element method seeks to determine a (finite-dimensional) function $\mathbf{p}_h \in V_q^h$ that satisfies Eq. (A6) for all $\mathbf{r}_h \in V_0^h$.

A Gaussian quadrature was used to approximate the double integral in Eq. (A6) and the resulting nonlinear system of equations for the nodal degrees of freedom was solved via Newton's method. A direct method was used to solve the linear system at each Newton iteration.

The time-dependent problem in Eqs. (A1) can be written as an initial value problem of the following form:

$$\frac{d\mathbf{p}}{dt} = \mathbf{h}[\mathbf{p}(t)], \quad t \in (0,T) \text{ with } \mathbf{p}(0) = \mathbf{p}_0. \tag{A8}$$

In our simulation, the method of Byrne and Hindmarsh[27] was used, which was designed for ''stiff'' initial value problems of the form

$$\frac{d\mathbf{Y}}{dt}=\mathbf{F}[\mathbf{Y}(t),t], \quad t\in(0,T) \ \text{ with } \ \mathbf{Y}(0)=\mathbf{Y}_0, \tag{A9}$$

where $\mathbf{F}:R^N\times R^{\mathrm{I}}\rightarrow R^N$ is continuous and satisfies a Lipschitz condition. Solutions to stiff differential equations develop over a wide range of time scales. Unlike fixed time-step integration techniques, the method of Byrne and Hindmarsh is a variable time-step method based on backward difference formulas of the order 1–5. In such variable time-step methods, the interpolation knots of interpolating polynomials must be distinct but they are otherwise arbitrary, allowing considerable flexibility in the size of the time step. It has changed six orders of magnitude during our calculations of equilibrium states.

An initial estimate for the solution at the nth time step, $\mathbf{y}_{n0}$ is determined from prior solutions $\mathbf{y}_{n-i}$, $(i=1,...,q)$, and is subsequently corrected using the residual function $\mathbf{y}_{\mathrm{n0}}-\mathbf{F}(\mathbf{y}_{n0},t_n)$. The order of interpolation q and the stepsize h are varied in response to estimates of local discretization error and user provided tolerances. The order of the method q is restricted to change in steps of $\pm$ 1 only.

[1] A. G. Luchaninov, A. V. Shil'nikov, L. A. Shuvolov, and I. Ju. Shipkova, Ferroelectrics **29**, 47 (1980).
[2] A. V. Turik and A. V. Chernobabov, Zh. Tekh. Fiz. **47**, 1944 (1977).
[3] W. Cao and L. E. Cross, Phys. Rev. B **44**, 5 (1991).
[4] W. Cao and L. E. Cross, Ferroelectrics **157**, 19 (1994).
[5] D. Vanderbilt and W. Zhong, Ferroelectrics **206**, 181 (1998).
[6] S. Nambu and D. A. Sagala, Phys. Rev. B **50**, 5838 (1994).
[7] H. L. Hu and L. Q. Chen, J. Am. Ceram. Soc. **81**, 492 (1998).
[8] K. Binder, Ferroelectrics **35**, 99 (1981).
[9] D. R. Tilly and B. Zeks, Ferroelectrics **134**, 313 (1992).
[10] W. L. Zhong, Y. G. Wang, P. L. Zhang, and B. D. Qu, Phys. Rev. B **50**, 698 (1994).
[11] Y. G. Wang, W. L. Zhong, and P. L. Zhang, Phys. Rev. B **51**, 5311 (1995).
[12] P. C. Hohenberg and B. I. Halperin, Rev. Mod. Phys. **49**, 435 (1977).
[13] V. A. Zhirnov, Zh. Eksp. Teor. Fiz. **35**, 1175 (1958) [Sov. Phys. JETP **35**, 822 (1959)].
[14] W. Cao and G. R. Barsch, Phys. Rev. B **41**, 11319 (1990).
[15] W. Cao, J. Phys. Soc. Jpn. **63**, 1156 (1993).
[16] M. J. Haun and L. E. Cross, Ferroelectrics **99**, 13 (1989).
[17] P. Würfel and I. P. Batra, Ferroelectrics **12**, 55 (1976).
[18] M. H. Frey and D. A. Payne, Phys. Rev. B **54**, 3158 (1996).
[19] T. Takeuchi, K. Ado, T. Asai, H. Kageyama, Y. Saito, C. Masquelier, and O. Nakamura, J. Am. Ceram. Soc. **77**, 1665 (1994).
[20] W. Cao and C. A. Randall, J. Phys. Chem. Solids **57**, 1499 (1996).
[21] C. Randall, N. Kim, J. P. Kucera, W. Cao, and T. Shrout, J. Am. Ceram. Soc. **81**, 677 (1998).
[22] I. P. Batra, P. Würfel, and B. D. Silverman, Phys. Rev. B **8**, 3257 (1973).
[23] J. F. Scott, H. M. Duiker, P. D. Beale, B. Pouligny, K. Dimmler, M. Parris, D. Butler, and S. Eaton, Physica B **150**, 169 (1988).
[24] K. A. Cliffe, ENTWIFE (release 6.3) Reference Manual: ENTWIFE, INITIAL DATA, and SOLVER DATA Commands, AEAT-0823, 1996.
[25] C. Johnson, ''Numerical solution of partial differential equations by the finite element method'' (Cambridge University Press, Cambridge, 1987).
[26] S. C. Brenner and L. R. Scott, *The Mathematical Theory of Finite Element Methods* (Springer, Berlin, 1994).
[27] D. Byrne and A. C. Hinmarsh, ACM Trans. Math. Softw. **1**, 71 (1975).